Micromagnetic model of noncollective magnetization reversal in ultrathin magnetic dots with in-plane uniaxial anisotropy

O. Fruchart,* B. Kevorkian, and J. C. Toussaint
Laboratoire Louis Néel (CNRS), BP166, 38042 Grenoble Cedex 9, France
(Received 1 August 2000; revised manuscript received 15 November 2000; published 6 April 2001)

In most magnetic systems the magnetization reversal is nonuniform, and is initiated in a so-called ''nucleation volume,'' whose dimensions are by far smaller than the total system volume. For simplicity reasons magnetization reversal theories are usually based on the assumption that coherent rotation occurs in this ''nucleation volume.'' In this approach, self-dipolar fields and exchange forces are obviously not well described, because in reality the nucleation volume is coupled with the rest of the system. In the case of ultrathin dots with in-plane uniaxial anisotropy, we could take into account dipolar fields and the exchange stiffness explicitly. The approximations used to derive analytical equations were suggested by experimental results on real dots. The model yields the nonuniform micromagnetic configuration of nucleation volumes. It predicts nucleation and reversal field values, as well as the field dependence of the energy barrier to be overcome to reverse the dot at finite temperature. The (negative) reversal field is found to increase with the dot thickness T and the volume magnetization M_s, and to decrease with the material anisotropy K. In the low-thickness limit, the reversal field H_r approaches the Stoner-Wohlfarth reversal field H_a with a law close to $1-|H_r/H_a| \sim M_s^{7/2}A^{-3/4}K^{-1}T^{3/2}$, where A is the exchange constant. The relevance of the approximations used is discussed and demonstrated by the good agreement found for all predictions between experiment and/or numerical calculations on the one hand and the model on the other hand.

DOI: 10.1103/PhysRevB.63.174418 PACS number(s): 75.60.−d, 75.40.Mg, 75.90.+w

I. INTRODUCTION

In the past two decades intense work has been devoted to the fabrication and study of magnetic thin and ultrathin films. New fundamental phenomena associated with well-defined two-dimensional (2D) structures (films) have been observed.[1–4] The attention is now focused as well on the study of systems of reduced lateral dimensions, ie., 1D (stripes)[5–9] and 0D (dots).[10–17] Several studies of fundamental interest arise from this further decrease of dimensionality: (1) The above-mentioned new phenomena also occur in 1D and 0D (and can even be enhanced), but with a different geometry, namely, with interfaces lying in the plane.[18,19] (2) New fundamental phenomena may arise, as observed for magnetoresistance enhancement due to Coulomb blockade.[20] (3) Qualitative or quantitative changes of micromagnetic behavior happen, the same way dipolar fields favor the in-plane alignment of magnetization for continuous thin films. These studies are also of importance for applications in the technological context of the ever-increasing integration demand for the fabrication of small devices and components.

The scope of the present paper lies in magnetic systems of reduced dimensions, more precisely in magnetization reversal processes in ultrathin flat dots with in-plane magnetization. On the one hand this study is of fundamental interest as it is related to the 50-year-old experimental search for coherent rotation (CR) of magnetization in small systems. On the other hand this study addresses an application concern, as devices like spin valves[21] and prospective topological bit recording media[22,11] require the use of such thin flat magnetic components. Studying the effect of the reduction of the dot thickness is of particular interest for spin valves. This is true for magnetic random access memories (MRAM's) as the integration via lateral size reduction requires the decrease of thickness of the magnetic layers in order to keep a reasonable thin-film-like aspect ratio. This is also of true for giant magnetoresistance (GMR) or tunneling magnetoresistance (TMR) magnetic head sensors, so that it may probe the stray fields arising from ever-narrower magnetic bits.

We recently reported experimental results demonstrating correlation between the decrease of the dot thickness and the increase of the ratio of coercive field over anisotropy field.[23–25] Here we propose an analytical model describing magnetization reversal in thin dots with in-plane uniaxial anisotropy. We explain below our motivation for proposing a new model by briefly reviewing available theories of magnetization reversal and showing that none of them are capable of describing the case of ultrathin dots with in-plane uniaxial anisotropy. The simplest model of magnetization reversal is CR, which was first proposed by Néel[26] and Stoner and Wohlfarth.[27] In this framework the reversal field H_r along the easy axis of magnetization is predicted to equal the anisotropy field H_a, where H_a includes the microscopic anisotropy (magnetocrystalline, magnetoelastic, interface) plus the shape anisotropy (aspect ratio). However, in real systems the most favorable magnetization configuration is generally not uniform (except for extremely small systems as was shown recently[17]) and H_r is considerably smaller than H_a, so that later on numerous nonuniform magnetization reversal processes have been proposed to account for the experimental small value of H_r. To this point it must be noted that even for one-dimensional problems there exists no general solution to micromagnetic equations, due to the long-range and nonlocal character of dipolar fields. Therefore, solutions can

be found only by introducing approximations or test functions. Many models had to be proposed to describe different types of systems, because the approximations introduced are valid in a limited range of parameters only.

Two types of theories were introduced. In the first type one assumes that some defects can be found in the samples. These defects are assumed to alter anisotropy and/or exchange constant values, or geometry. The defects may decrease the nucleation field as compared to the anisotropy field (''soft'' defects) or explain the value of propagation fields (pinning defects). We do not consider such processes in the present paper, as we are interested in systems having no significant defects. To the contrary, we wonder what intrinsic magnetization reversal mechanisms may occur apart from coherent rotation that may lead to a reversal field smaller than the anisotropy field. We therefore turn to the other type of theories, assuming no defects. Due to the complexity of micromagnetic equations, only highly symmetrical collective reversal modes could be investigated analytically. These processes may be relevant for systems of very small size or, more generally, for soft-material systems with a shape of high symmetry.[28] Such theories include curling[29–32] and buckling[30] or extensions made to investigate zero-field[33,34] and field-dependant[35] states of more or less flat dots made of a soft material. More recently a variational method was introduced by Cowburn and Welland in the case of square dots made of soft material.[36] These authors describe a nonuniform magnetization configuration in a dot as the superposition of a uniform magnetization state and low-order perturbations with ''leaf'' or ''flower'' symmetry. For reasonably small dots a remarkable agreement between the model and numerical calculations is found.[36,37] The resulting magnetization configuration is, however, still collective as only perturbations of high symmetry are considered. This model may therefore be relevant only to describe flat dots made of soft material and with negligible thermal activation, which we know from theory and experiments to adopt such collective static modes.[33–35] Finally, no external fields are taken into account in these models in their present state, so that only remanent static magnetization configurations are predicted, and hysteretic effects can only be extrapolated. We finally mention an attempt to derive a theory for anisotropic flat dots. Chui and Ryzhov[38] proposed a trial micromagnetic configuration for a flat rectangular dot under zero applied field. The edge condition $\mathbf{m}\cdot\mathbf{n}=\mathbf{0}$ mimics dipolar energy minimization, whereas the configuration in the bulk of the dot satisfies exactly micromagnetic equations with no dipolar fields. The authors show that the trial configuration is close to the one issued from numerical calculation performed on a dot *with a certain thickness*. In fact the proposed trial configuration is thickness independent, and therefore should be neither adequate for ''large'' thickness (the edge condition $\mathbf{m}\cdot\mathbf{n}=\mathbf{0}$ is correct but volume charges should then be taken into account) nor for ''small'' thickness (the $\mathbf{m}\cdot\mathbf{n}=\mathbf{0}$ edge condition is too strong; the dot configuration is rather close to uniform).

To our knowledge there exists no realistic analytical reversal model in flat dots with in-plane uniaxial anisotropy and with dimensions well above λ_{ex} and λ_{Bl}. By in-plane uniaxial anisotropy, we mean in-plane magnetization and a uniaxial anisotropy of microscopic origin between two in-plane directions. Indeed, in the presence of anisotropy the magnetization is expected to reverse by a nucleation-propagation process. This is confirmed experimentally as nucleation volumes, as determined by aftereffect measurements, are by far smaller than the system size.[6,39] Therefore, highly symmetrical collective modes should not account for the observed H_r reduction. How does one describe magnetization reversal in such dots? One sometimes assumes that coherent rotation occurs in a small nucleation volume, and the aspect ratio of the dot is then invoked to estimate the dipolar contribution to an effective magnetic anisotropy of the nucleation volume. This approach may be very misleading as (i) the exchange is not taken into account whereas the magnetization configuration is obviously nonuniform and (ii) dipolar fields are generally nonuniform in samples, so that the relevance of the aspect ratio that is related to the *mean value* of H_d over the dot volume is doubtful. The latter argument is particularly acute in the present case of thin flat dots as the magnetic poles are then located on edges of the dot only. Therefore self-dipolar fields are very intense in the vicinity of edges and very weak in the center of the dot, because of the short range of dipolar fields in 2D systems.[23] To the contrary, the approach followed in the present model is to take into account the exchange contribution and the local dipolar fields, and to derive explicitly the micromagnetic configuration of a nucleation volume growing near an edge, for any applied field and up to the reversal field.

The principle of the model and the approximations introduced are given in Sec. II. The equations are explicitly derived and solved in Sec. III. We show that the model predicts the reversal field value, the reversible contribution before the reversal, and the micromagnetic configuration of nucleation volumes, as well as the field dependence of the energy barrier preventing the reversal. Some examples of the model outputs are given in Sec. IV. Finally, Sec. V is devoted to comparing the model with numerical calculations and experiments. The approximations used, the relevance of the model, and its micromagnetic consequences are finally discussed.

II. DESCRIPTION OF THE MODEL

A. Dimensionless units

In the following we will use dimensionless units for the sake of concision. Uppercase letters stand for dimensional variables whereas lowercase letters stand for dimensionless variables. First, all lengths are expressed in terms of $\sqrt{A/K}$ where A is the exchange constant, and K is the in-plane second-order anisotropy constant of the dot material, including all microscopic anisotropy sources (magnetocrystalline, magnetoelastic, and interface). Any dimensionless length l is related to the real length L like $l=L\sqrt{K/A}$. If we use the definitions of the Bloch wall width $\lambda_{Bl}=\pi\sqrt{A/K}$ and the exchange length $\lambda_{ex}=\pi\sqrt{2A/\mu_0 M_s^2}$, we have in dimensionless units: $\lambda_{Bl}=\pi$ and $\lambda_{ex}=\pi\sqrt{2}/m$. Second, there are two ways of reducing magnetic fields H and the volume magnetization M_s. The symmetrical way consists in reducing both

variables with $\sqrt{K/\mu_0}$. We will denote $h=H\sqrt{\mu_0/K}$ and $m=M_s\sqrt{\mu_0/K}$ as the corresponding dimensionless variables. The nonsymmetrical way consists in reducing H with the anisotropy field $H_a=2K/\mu_0 M_s$ and M_s with M_s itself. We will denote $\tilde{h}=H\mu_0 M_s/2K$ as the field reduced in this way (and $\tilde{m}=1$ does not appear anymore). The symmetrical reduction is more explicit for dipolar field calculations as m still shows up explicitly. The nonsymmetrical reduction is more convenient for analyzing magnetization reversal, as $\tilde{h}=-1$ means coherent rotation. However, in both reduction systems, the characteristic magnetic length scales are identical. Finally, the energy density of a second-order anisotropy system under an external field applied parallel to the easy axis of magnetization is written

$$e_V=\sin^2\omega+(\nabla\omega)^2-mh\cos\omega \tag{1}$$

$$=\sin^2\omega+(\nabla\omega)^2-2\tilde{h}\cos\omega, \tag{2}$$

where ω is the angle between **M** and the easy axis. Along the entire paper we will often refer to the experimental case of 1-nm-thick (110)Fe dots,[25] for which $M_s=1.73\times10^6$ A m^{-1}, $K=4.76\times10^5$ J m^{-3}, $A=2\times10^{-11}$ J m^{-1}, $\lambda_{Bl}=20.4$ nm, and $\lambda_{ex}=10.2$ nm. To give an order of magnitude to the reader, $m=2.81$ and $\lambda_{ex}=1.58$ in this case.

B. Approximations used

In the model, we make use of both power series expansion and micromagnetic approximations. The expansion approximation consists of an exact power series expansion of microscopic magnetic torques up to the fifth order, in terms of the magnetization angle ω. The choice and the consequences of the order of expansion will be discussed in the last section. Here, we focus on the micromagnetic approximations, which are based on the analysis of experiments performed on ultrathin dots 200 nm wide made of Fe films with in-plane anisotropy.[40] The present section is devoted to introducing these approximations and discussing the physical ground of their relevance.

We showed experimentally that for such dots the nucleation volumes are approximately 100 times smaller than the total volume of the dot.[24] This demonstrated that magnetization reversal is *not* coherent. The reversal is therefore expected to proceed in two steps: First, a small nucleation volume reverses. Second, the magnetization of the entire dot is reversed by a fast domain wall motion process. Besides, dipolar fields are short ranged in 2D systems[23] so that self-demagnetizing fields $\mathbf{h}_d$ are strongly nonuniform inside the dot. These fields nearly vanish near the center of the dot and are strong only in the close vicinity of the edges that are perpendicular to the magnetization direction. The nucleation volumes are therefore expected to be located in the vicinity of these edges. In micromagnetics corners may help or hinder magnetization reversal, depending on the situation. We assume that corners hinder magnetization reversal in our case, so that the reversal should be triggered near edges but away from corners. The proof for this assumption comes from numerical micromagnetic simulations, whose results will be detailed in the discussion section. As we already mentioned above, dipolar fields are short ranged so that the micromagnetic configuration of the nucleation volume should be characteristic of the neighboring edge only, because the influence of corners and of the opposite edge are comparatively very weak. It should finally be added that the influence of corners and other edges is not mediated to the nucleation volume via exchange, as the in-plane length scale of the exchange length, the domain-wall width, and that of the nucleation volume are small as compared to the dot lateral size. In this respect, the present situation is very different from that commonly encountered in the case of soft material. All this leads to the first micromagnetic approximation, which is of a geometrical nature: the dot is replaced in the model by a half-infinite slab whose edge is perpendicular to the easy axis of magnetization, and a translation symmetry along this edge is assumed (Fig. 1).

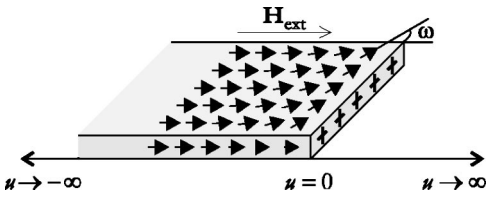

FIG. 1. Schematic cross-section view of the slab with external field applied perpendicular to the edge and parallel to the easy axis of magnetization. In this geometry the so-called surface magnetic poles are located on the edge (+). The field is positive in the figure. Negative values will be applied to reverse the dot magnetization.

The second micromagnetic approximation is derived from the observation that the experimental in-plane angular dependence of the reversal field $h_r(\theta)$ is very close to the predictions of CR.[40] This indicates that even in the vicinity of an edge, the influence of demagnetizing fields is weak. This implies that the magnetization state of nucleation volumes is close to uniform, even just before the nucleation event occurs. We accordingly assumed that only edge magnetic poles contributed to self-dipolar fields, not volume poles $\nabla\cdot\mathbf{m}$. Then, as dipolar effects are very short ranged in 2D systems, dipolar fields coming from the neighboring edge charges apply only to a small fraction of the nucleation volume, more precisely to the fraction that is in the immediate vicinity of the edge. Let us recall that the length scale of a nucleation volume in our case is at least λ_{ex} as exchange forces forbid any rapid magnetization rotation on a length scale smaller than λ_{ex}, whereas the range of dipolar fields is related to the dot thickness (t). The demagnetizing effect was accordingly taken into account as a demagnetizing torque Γ_d acting on the edge spin of the half-infinite slab, and Γ_d is estimated by integrating the microscopic self-dipolar torque $\gamma_d=\mathbf{m}\times\mathbf{h}_d$ from the edge to infinity. This is the second important micromagnetic approximation. Several remarks must be made. First, integrals of torques converge rapidly even in the case of infinite lines of charges, instead of diverging in the case of energy integrals. Second, $t\ll\lambda_{ex}$ appears naturally as the criteria of validity for this ''torque approximation.'' Third, the relevance of the concept of the edge torque is supported by

the results of Rave *et al.* These authors recently discussed and simulated the relevance of edge torques to account for the effect of demagnetizing fields acting on a length scale smaller than λ_{ex}.[41]

Finally a third micromagnetic approximation is introduced. This approximation is also derived from the fact that $t \ll \lambda_{ex}$: the magnetization cannot be reoriented away from in plane in the vicinity of edges. Besides, the magnetization can be considered as uniform along the thickness of the dot because $t \ll \lambda_{ex}$ and $t \ll \lambda_{Bl}$. As a result, the magnetization in the half-infinite slab can be written as

$$\mathbf{m}(u) = m[\mathbf{i} \cos \omega(u) + \mathbf{j} \sin \omega(u)]. \tag{3}$$

$u \in [-\infty; 0]$ is the distance between the considered point and the edge. $\omega(u)$ is the in-plane angle between the magnetization vector and the easy axis of magnetization (see Fig. 1).

Let us summarize the three micromagnetic approximation that we introduced

(i) The magnetization lies in the plane and does not vary along the thickness of the film.

(ii) The geometry is restricted to a half-infinite slab whose edge is perpendicular to the easy axis of magnetization, and a translation symmetry along the edge is assumed.

(iii) The dot self-dipolar fields are taken into account as an edge torque, whose value is calculated by integrating the microscopic dipolar torque from the edge of the slab to infinity.

Let us also recall that, in addition to these approximations, we will in the following proceed to a series expansion of microscopic magnetic torques, including all terms up to the fifth order.

C. Principle of the model

Let us now briefly describe the principle of the model in the framework of the three micromagnetic approximations described above. The micromagnetic configuration inside the slab is determined by the minimization of the anisotropy, Zeeman, and exchange energies (Euler's equation). This configuration can be described analytically using a wall-type expression,[42,43] provided that we set the magnetization rotation at the edge to a value fixed *a priori*, $\omega_0 = \omega(u=0)$. The edge magnetic pole is then $\cos(\omega_0)$, from which $\mathbf{h}_d(u)$ is calculated, leading to the evaluation of Γ_d. Finally, Euler's equation is applied at the edge (Brown's condition); namely, the exchange-induced torque Γ_{ex} and the dipolar torque Γ_d must compensate each other, so that the spin at the edge is under equilibrium:

$$\Gamma_{ex} + \Gamma_d = 0. \tag{4}$$

The possible equilibrium values of ω_0 are finally determined self-consistently, by solving Eq. (4).

III. MODEL SOLVING

A. Wall profile

We restrict ourselves to dots with a second-order microscopic in-plane anisotropy energy; i.e., we use Eq. (2). The procedure is the following. The dot is first saturated with high positive values of $\tilde{h}$. Then smaller positive and finally negative values of $\tilde{h}$ are applied to reverse the magnetization of the dot. Equation (2) can be written

$$e_v = 4(1+\tilde{h})\left[\left(\frac{d\theta}{d\eta}\right)^2 + \sin^2\theta + k_2 \sin^4\theta\right], \tag{5}$$

with $k_2 = -1/(1+\tilde{h})$, $\theta = \omega/2$, and $\eta = u\sqrt{1+\tilde{h}}$. The solution to Eq. (5) is the equation of a wall in a fourth-order anisotropy material, which was solved analytically.[42,43] Using this expression and switching back to variables u and ω one finds

$$\omega = \pi - 2\arctan\left\{\sqrt{\frac{-\tilde{h}}{1+\tilde{h}}}\cosh[\sqrt{1+\tilde{h}}(u-u_1)]\right\}. \tag{6}$$

Here ''cosh'' is the hyperbolic cosine function, and u_1 is a positive integration constant which determines the location of the wall ($u_1 \gg 1$ for a small edge rotation). Besides, we have broken arbitrarily the left-right symmetry by choosing a nonuniform solution with $\omega_0 > 0$. The single-domain state is obtained in the limit $u_1 \to +\infty$, in which case $\omega_0 = 0$, and thus $\omega(u) = 0, \forall u$.

B. Exchange-induced torque

The exchange-induced torque acting on the edge spin is expressed as

$$\Gamma_{ex} = -2\left.\frac{d\omega}{du}\right|_{u=0}. \tag{7}$$

To this point, it is useful to go back to Euler equation, rather than to use directly Eq. (6). Indeed, the bulk Euler condition connects the microscopic torque with the anisotropylike microscopic energy density:

$$\frac{d\theta}{d\eta} = \sqrt{e_a(\theta)}, \tag{8}$$

where the integration constants vanish in the case of the half-infinite slab, $e_a(-\infty) = 0$ and $d\theta/d\eta(-\infty) = 0$, and with the notation of Eq. (5), $e_a(\theta)$ varies like $\sin^2\theta + k_2 \sin^4\theta$. Switching back to the variables ω and u, the right-hand side of Eq. (8) can be straightforwardly expanded in a power series as a function of ω. Performing the exact expansion up to the fifth order and using Eq. (7), one finally finds

$$\Gamma_{ex} = -2\omega_0\sqrt{1+\tilde{h}}\left\{1 - \frac{1}{2}\left(\frac{1}{3} + \frac{1}{1+\tilde{h}}\right)\left(\frac{\omega_0}{2}\right)^2 + \frac{1}{2^3}\left[\frac{1}{15} + \frac{2}{1+\tilde{h}} - \frac{1}{(1+\tilde{h})^2}\right]\left(\frac{\omega_0}{2}\right)^4 + O(\omega_0^6)\right\}. \tag{9}$$

C. Demagnetizing torque

Let us recall that we neglect volume magnetic charges, so that the demagnetizing fields arise from surface magnetic

charges only (i.e., from the edges). Besides, for simplicity the average demagnetizing field over the dot thickness t was approximated by the demagnetizing field value calculated in the center of the film ($z=t/2$), namely,

$$h_{\mathrm{d}}(u)=\frac{m\cos(\omega_0)}{\pi}\arctan\left(\frac{t}{2u}\right). \tag{10}$$

Using this expression, the microscopic (i.e., local) demagnetizing torque can be expressed as

$$\gamma_{\mathrm{d}}(u)=-\frac{m^2}{\pi}\cos(\omega_0)\sin(\omega)\arctan\left(\frac{t}{2u}\right). \tag{11}$$

The edge demagnetizing torque is finally given by

$$\Gamma_{\mathrm{d}}=\int_{-\infty}^{0}\gamma_{\mathrm{d}}(u)\,du. \tag{12}$$

Note that $u<0$ in Eqs. (10)–(12), so that we indeed have a demagnetizing field ($h_d<0$) and demagnetizing torque [$\gamma_{\mathrm{d}}(u)>0$].

In order to get a series expansion of Γ_{d} as a function of ω_0, we first expand $\sin\omega$ as a function of ω_0 with u-dependent coefficients, and then proceed to the integration of these coefficients following Eqs. (11) and (12). The simplest way to do this is to perform, as an intermediate step, the expansion of $\sin\omega$ as a function of the small quantity $e^{\eta-\eta_1}$, with $\eta_1=u_1\sqrt{1+\tilde{h}}$ [see also Eq. (6)]. As a second step, the integration of Eq. (12) is performed, yielding an expression with integral powers of $e^{-\eta_1}$. Finally, $e^{-\eta_1}$ is in turn expanded in terms of ω_0. This two-step expansion is relevant because $e^{-\eta_1}$ is of the order of ω_0.

Reversing Eq. (6), one finds

$$\sin\omega=\frac{2\alpha\cosh(\eta-\eta_1)}{1+\alpha^2\cosh^2(\eta-\eta_1)}, \tag{13}$$

where $\alpha=\sqrt{-\tilde{h}/(1+\tilde{h})}$. The exact expansion of Eq. (13) to the fifth order is

$$\sin\omega=\frac{4}{\alpha}e^{\eta}e^{-\eta_1}\left[1-\left(1+\frac{4}{\alpha^2}\right)e^{2\eta}e^{-2\eta_1}+\left(1+\frac{12}{\alpha^2}+\frac{16}{\alpha^4}\right)e^{4\eta}e^{-4\eta_1}+O(e^{6\eta}e^{-6\eta_1})\right]. \tag{14}$$

With a view to proceeding to the integration in Eq. (12), it is now necessary to evaluate the series of integrals

$$I_k(\tilde{h})=-\int_{-\infty}^{0}e^{k\eta}\arctan\left(\frac{t}{2u}\right)du \tag{15}$$

where k has positive integral values among $\{1,3,5\}$. For clarity, we will in the following omit to write the dependence of I_k upon $\tilde{h}$. Using the variables $\beta=t/2$ and $\mu_k=k\sqrt{1+\tilde{h}}$, the I_k function is expressed as

$$I_k=\frac{1}{\mu_k}\left(\frac{\pi}{2}-\beta\int_0^{+\infty}\frac{e^{-u\mu_k}}{u^2+\beta^2}du\right) \tag{16}$$

and evaluated using the following expression of the integral[44]:

$$\int_0^{+\infty}\frac{e^{-u\mu_k}}{u^2+\beta^2}du=\frac{1}{\beta}[\mathrm{ci}(\beta\mu_k)\sin(\beta\mu_k)-\mathrm{si}(\beta\mu_k)\cos(\beta\mu_k)]. \tag{17}$$

ci and si are sine and cosine integral functions, respectively. These functions can be evaluated numerically using the following expansions[44]:

$$\mathrm{ci}(x)=\mathrm{C}+\ln x+\sum_{k=1}^{\infty}(-1)^k\frac{x^{2k}}{2k(2k)!}, \tag{18}$$

$$\mathrm{si}(x)=-\frac{\pi}{2}+\sum_{k=1}^{\infty}(-1)^{k+1}\frac{x^{2k-1}}{(2k-1)(2k-1)!}. \tag{19}$$

After this integration, the demagnetizing torque is written the following way, after Eqs.(12) and (14):

$$\Gamma_{\mathrm{d}}=\frac{4m^2}{\alpha\pi}\cos(\omega_0)\times\left[e^{-\eta_1}I_1-e^{-3\eta_1}\left(1+\frac{4}{\alpha^2}\right)I_3+e^{-5\eta_1}\left(1+\frac{12}{\alpha^2}+\frac{16}{\alpha^4}\right)I_5\right]. \tag{20}$$

The final step is to express $e^{-\eta_1}$ as a series expansion of ω_0. Equation (6) yields ω_0 as a function of η_1. This relation can be reversed, yielding a binomial relation, with two positive roots $e^{-\eta_1}$ and e^{η_1}. The smaller root must be connected with $e^{-\eta_1}$ because $\eta_1>0$, and one finds

$$e^{-\eta_1}=\frac{1}{\alpha}\cot\frac{\omega_0}{2}-\sqrt{\frac{1}{\alpha^2}\cot^2\frac{\omega_0}{2}-1}. \tag{21}$$

Finally, after evaluation of the series expansions of Eq. (21), $\cos\omega_0$, I_1, I_3 and I_5 as a function of ω_0, Eq. (20) can be fully exactly expanded to the fifth order:

$$\Gamma_{\mathrm{d}}=\left\{\frac{I_1}{2}\left(\frac{\omega_0}{2}\right)+\left[-\frac{1}{6}(5I_1+3I_3)+\frac{\alpha^2}{8}(I_1-I_3)\right]\left(\frac{\omega_0}{2}\right)^3+\left[\frac{1}{30}(2I_1+15I_3+15I_5)+\frac{\alpha^2}{8}(-I_1-2I_3+3I_5)+\frac{\alpha^4}{32}(2I_1-3I_3+I_5)\right]\left(\frac{\omega_0}{2}\right)^5+O(\omega_0^7)\right\}\frac{4m^2}{\pi}. \tag{22}$$

D. Equilibrium states

The equilibrium states are determined by equilibrium of the spin at the edge [Eqs. (4), (9), and (22)]. Apart from the trivial solution $\omega_0=0$ (single-domain state), the equilibrium positions are the roots of binomial

$$A\left(\frac{\omega_0}{2}\right)^4+B\left(\frac{\omega_0}{2}\right)^2+C=0, \tag{23}$$

with the following expression of the coefficients:

$$A=\frac{m^2}{\pi}\left[\frac{2}{15}(2I_1+15I_3+15I_5)+\frac{\alpha^2}{2}(-I_1-2I_3+3I_5)+\frac{\alpha^4}{8}(2I_1-3I_3+I_5)\right]-\frac{1}{2}\sqrt{1+\tilde{h}}\times\left[\frac{1}{15}+\frac{2}{1+\tilde{h}}-\frac{1}{(1+\tilde{h})^2}\right],$$

$$B=\frac{m^2}{\pi}\left[-\frac{2}{3}(5I_1+3I_3)+\frac{\alpha^2}{2}(I_1-I_3)\right]+2\sqrt{1+\tilde{h}}\left(\frac{1}{3}+\frac{1}{1+\tilde{h}}\right),$$

$$C=\frac{2m^2}{\pi}I_1-4\sqrt{1+\tilde{h}}. \tag{24}$$

The two roots are

$$\left(\frac{\omega_0^{\pm}}{2}\right)^2=\frac{-B\pm\sqrt{\Delta}}{2A}, \tag{25}$$

with

$$\Delta=B^2-4AC. \tag{26}$$

As by convention $\omega_0>0$ and including the single-domain solution $\omega_0=0$, there exists at most three equilibrium solutions for the nonreversed state (either stable or unstable), depending on the external field value $\tilde{h}$. The state with the largest ω_0 is associated with the barrier to be overcome to reverse the magnetization, so that it is unstable. Besides, $\Gamma_{ex}-\Gamma_d$ is a continuous function versus ω, so that successive equilibrium states are successively stable and unstable, with decreasing values of ω_0. This allows us to describe qualitatively the three different situations that can be encountered.

(i) There are three positive solutions, namely, $\omega_0=0$, $\omega_0^-\!>\!0$, and $\omega_0^+\!>\!\omega_0^-$. The only stable equilibrium state is then ω_0^- and the magnetization configuration is nonuniform (NU) near the edge. This occurs for $\Delta>0$ and $(\omega_0^-)^2\!>\!0$.

(ii) There are two positive solutions only, namely, $\omega_0=0$ and $\omega_0^+\!>\!0$. The only stable equilibrium state then corresponds to $\omega_0=0$ [single-domain (SD) state]. This occurs for $\Delta>0$, $(\omega_0^-)^2\leqslant 0$, and $(\omega_0^+)^2\!>\!0$.

(iii) The only solution is $\omega_0=0$ and is unstable. This means that the magnetization has already reversed. This occurs in two cases, either $\Delta<0$ or $\Delta\geqslant 0$ and $(\omega_0^+)^2\leqslant 0$.

We observe that there is at most one stable equilibrium solution. The reversal field $\tilde{h}_r$ is the field at which this single stable solution vanishes. Depending on the situation (NU or SD; see above) $\tilde{h}_r$ is determined by ω_0^+(unstable) $=\omega_0^-$(stable) or ω_0^+(unstable)$=0$(stable), respectively. In the NU case, h_n is found by solving the equation $\omega_0^+=0$.

E. Energy barriers

In this section we calculate the height of the energy barrier preventing magnetization reversal. This might be of use to gain insight into the thermal activation behavior of the dot.

As explained above, the model was solved based on torque equations. One can also use the picture of a system with a single degree of freedom ω_0 in a $[0;\pi]$ energy landscape. In this picture, the bottom of the energy well stands for the stable state, whereas the top of the barrier preventing magnetization reversal stands for the unstable state. The height of the barrier equals the work produced by an operator applying a torque Γ_{op} on the spin at the edge, in order to drive it from the stable position ω_0^s to the unstable position ω_0^+, under quasistatic conditions: $\Gamma_d+\Gamma_{ex}+\Gamma_{op}=0$. The barrier height is therefore

$$W_{op}=-\int_{\omega_0^s}^{\omega_0^+}(\Gamma_d+\Gamma_{ex})d\omega_0. \tag{27}$$

ω_0^s stands for the stable equilibrium solution, either ω_0^- (NU) or 0 (SD). One finds after straightforward integration of Eq. (23)

$$W_{op}=[\xi(\omega_0)]_{\omega_0^s}^{\omega_0^+}, \tag{28}$$

with

$$\xi(\omega_0)=-\frac{A}{3}\left(\frac{\omega_0}{2}\right)^6-\frac{B}{2}\left(\frac{\omega_0}{2}\right)^4-C\left(\frac{\omega_0}{2}\right)^2. \tag{29}$$

For the stable state of the SD case $\omega_0^s=0$, so that $\xi(\omega_0^s)=0$. For the stable state of the NU case ω_0 is a root of binomial (23), so that $\xi(\omega_0=\omega_0^{\pm})$ can be expressed in terms of *A*, *B*, and *C* only. It is now necessary to treat the NU and SD cases separately.

In the NU case Eq. (28) boils down to the following exact expression:

$$W_{op}=\frac{\Delta^{3/2}}{6A^2}. \tag{30}$$

Magnetization reversal occurs when Δ vanishes (see *NU state* in the previous paragraph). Δ can be expanded to first order, as the first derivative of Δ generally does not vanish in $\tilde{h}=\tilde{h}_r$: $\Delta\sim\tilde{h}-\tilde{h}_r$. Then, we get from Eq. (30) the first-order expansion $W_{op}\sim(\tilde{h}-\tilde{h}_r)^{3/2}$. This shows that the α exponent used in thermal activation theory equals 1.5 in the case of a nonuniform state with **h** applied exactly perpendicular to the edge.

In the SD case, magnetization reversal occurs when ω_0^+ vanishes (see *SD-state* in the previous paragraph). Equation (28) can be expanded in terms of ω_0^+. The leading order of the expansion is

$$W_{\mathrm{op}} \approx \frac{B}{2}(\omega_0^+)^4. \tag{31}$$

$\tilde{h}=\tilde{h}_{\mathrm{r}}$ is reached when C changes of sign [see Eq. (25) and the discussion below]. In general B does not vanish in $\tilde{h}=\tilde{h}_{\mathrm{r}}$, so that Eqs. (25) and (26) can be expanded straightforwardly, showing that $(\omega_0^+)^2$ varies linearly with $\tilde{h}-\tilde{h}_{\mathrm{r}}$ just before the reversal, and thus $W_{\mathrm{op}} \sim (\tilde{h}-\tilde{h}_{\mathrm{r}})^2$. From this and from Eq. (31) we infer that the exponent α equals 2 in the SD case.

IV. MODEL QUANTITATIVE RESULTS

A. Numerical application to 1-nm-thick dots

Theory is more flexible than experiment as each parameter can be varied one at a time to evaluate its influence on magnetization reversal. Such a step-by-step comparison is not possible with real samples, where, for instance, thickness and anisotropy cannot be chosen independently because of the interplay of interface, magnetoelastic, and volume anisotropies. The primary purpose of the torque model is to investigate the intrinsic influence of thickness, so that the examples given below were computed for different thicknesses but for fixed anisotropy. An advantage of not presenting the model's results in a $(t,\tilde{h})$ graph using an experimental $H_{\mathrm{a}}(t)$ law is that the results presented here do not depend on a particular sample and are therefore more general. The reader should, however, keep in mind that a comparison of such a graph computed in units reduced with respect to one given anisotropy is in principle possible for one thickness only, because of the thickness-anisotropy experimental interplay.

The equations $\Delta=0$, $\omega_0^-=0$, and $\omega_0^+=0$ were solved numerically, using the experimental values $H_{\mathrm{a}}=0.55$ T and $M_{\mathrm{s}}=1.73\times10^6$ A m^{-1}.[25] Stable and unstable equilibrium state curves for different thicknesses are displayed on a $(\tilde{h},\omega_0)$ plot in Fig. 2. For a given $\tilde{h}$ the number and numerical values of equilibrium states are determined graphically by the intersection of these curves with a vertical line. The nucleation field value $\tilde{h}_{\mathrm{n}}$ and the reversal field value h_{r} were determined numerically using this type of diagram. Both fields are plotted versus thickness on Fig. 3. Note that here ''nucleation field'' $\tilde{h}_{\mathrm{n}}$ bears a micromagnetic meaning; i.e., h_{n} is the field at which the SD state becomes a NU state.[45] It should not be confused with the reversal field $\tilde{h}_{\mathrm{r}}$, at which a ''nucleation event'' (in the viscosity measurement meaning, i.e., the thermally activated reversal of a small volume) triggers magnetization reversal. We see in Fig. 3 that below a critical thickness t_{c} the magnetization configuration is always SD up to $\tilde{h}_{\mathrm{r}}$ (in that case $\tilde{h}_{\mathrm{n}}=\tilde{h}_{\mathrm{r}}$), whereas for $t>t_{\mathrm{c}}$ the magnetization configuration is successively SD, NU, and then reversed, as $\tilde{h}$ is decreased towards -1 (in the latter case $\tilde{h}_{\mathrm{n}}>\tilde{h}_{\mathrm{r}}$). The transition from a SD state to a NU state is of second order; i.e., ω_0 switches continuously and reversibly from zero to positive values at $\tilde{h}_{\mathrm{n}}$. On further decrease of $\tilde{h}$, ω_0 monotonously increases up to ω_0^{r} at $\tilde{h}_{\mathrm{r}}$. Although results concerning one (H_{a},m) set only are given here, the same qualitative t dependence was found for any values of m and H_{a}. We found, in accordance with intuition, that t_{c} and $\omega_0^{\mathrm{r}}|_{t=\mathrm{Cte}}$ increase if M_{s} increases or H_{a} decreases, and that $d\omega_0^{\mathrm{r}}/dt>0$ for $t>t_{\mathrm{c}}$.

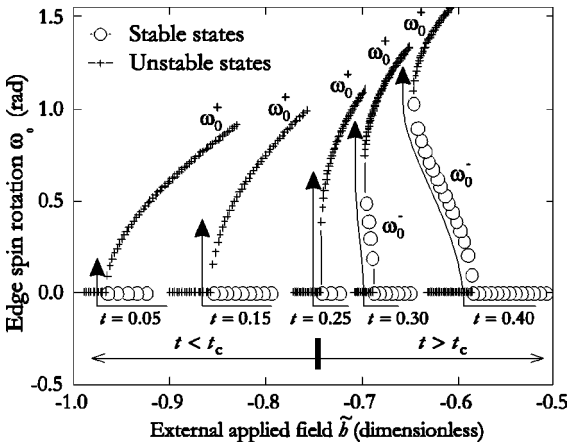

FIG. 2. Stable (○) and unstable (+) equilibrium states in a $(\tilde{h},\omega_0)$ plot, as predicted by the model for $m=2.81$ and for thicknesses ranging from 0.05 to 0.4 (dimensionless units). ω_0 is the rotation of the spin located at the very edge of the half-infinite slab.

B. Comparison with numerical calculations

Our numerical approach is based on solving dissipating Landau-Lifschitz-Gilbert micromagnetic equations and using a fast Fourier transform (FFT) procedure to evaluate dipolar fields.[46,47] Special care was devoted to track numerical artifacts and to simulate model systems to validate the approach,

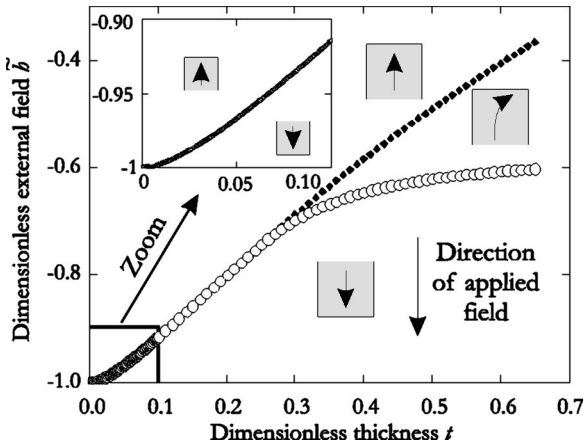

FIG. 3. Micromagnetic state of a half-infinite slab as predicted by the model. Open dots stand for reversal fields and solid diamonds stand for nucleation fields. An enlargement of the small thickness area is shown in the inset.

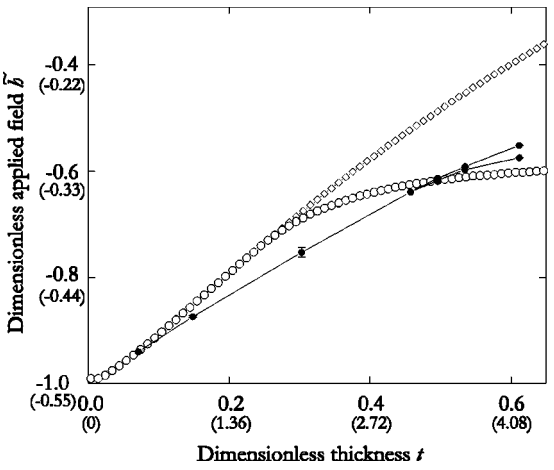

FIG. 4. Nucleation and reversal fields (diamonds and dots, respectively) vs slab thickness: predicted by the model (open symbols) and yielded by numerical calculations of a half-infinite slab (solid dots) ($m=2.81$ in both cases). Dimensionless units were converted into real units on both axes for the case of experimental 1-nm-thick Fe dots (see parentheses: thickness in nm and field in T). Error bars are related to the field step used in the calculation.

so that we are confident that the error bars of numerical calculations are smaller than those induced by the approximations used in the model. Accordingly, any discrepancy between calculations and the torque model will be ascribed to the latter in the following. The calculations were performed using the parameters of experimental 1-nm-thick dots: $H_a=0.55$ T and $M_s=1.73\times10^6$ A m^{-1}.[25]

Two major approximations were used in the model. The first one is the torque approximation. The second one is the geometric approximation, namely, the replacement of a finite-size dot by a half-infinite slab. Numerical calculations allowed us to probe the relevance of each approximation independently, as reported below.

In a first step, we assess the relevance of the edge torque approximation. For doing this, we numerically simulated the magnetization reversal process in a half-infinite slab with a translation symmetry parallel to the edge, the magnetization being a 3D vector. For each value of the external applied field we used the following procedure in order to get rid of the numerical left-right symmetry-breaking problem, but at the same time to be able to predict a value for the nucleation field, i.e., the field at which a system ceases to be uniformly magnetized: in a first step the external field is misaligned by 0.1° with respect to the easy axis of magnetization, and an equilibrium configuration is calculated. In this configuration ω_0 never exactly equals 0. In a second step we use this configuration as a starting point and calculate the equilibrium configuration under a perfectly aligned external field. The nucleation field has not yet been reached if the solution relaxes towards uniform magnetization with $\omega_0=0$. We found that numerical calculations and the model yield identical *qualitative* results (Fig. 4): below a critical thickness the system is always uniformly magnetized under any applied field. Above the critical thickness the system can be uniformly or nonuniformly magnetized, depending on the external field value. This leads to a distinct nucleation field $\tilde{h}_n$ and reversal field $\tilde{h}_r$. The *quantitative* agreement is very good in the ultrathin regime. However, the regime over which a NU magnetization state can exist lies at the verge of the model validity domain, for the set of parameters used for the comparison (a more detailed comparison will be found in Sec. V). The slab geometry is identical in these numerical calculations and in the analytical model. The difference lies in the fact that the numerical calculations do not make use of the torque approximation nor of power series expansions. This proves the relevance of the torque approximation and the low-order expansions used in the analytical model in the limit of ultrathin dots.

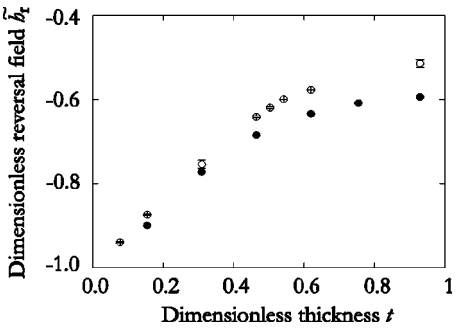

FIG. 5. Reversal field value vs thickness, yielded by numerical calculations performed on half-infinite slabs (open symbols) and square-shaped dots with a 200-nm edge (solid symbols), both using $m=2.81$. Error bars correspond to the field step used in the calculation.

In a second step, we assess the relevance of the geometrical approximation. For this purpose, we compared the simulations previously discussed, performed on a half-infinite slab, with simulations performed on a square-shaped dot with a 200-nm edge, the edges being parallel to the in-plane easy and hard axes of the film. In both cases the thickness is 1 nm and the magnetization is described by a 3D vector **m**. The grid spacing was chosen equal to 3.125 nm, smaller than $\lambda_{ex}=10.2$ nm and $\lambda_{Bl}=20.4$ nm. Both calculations yield very similar $\tilde{h}_r$ values as shown in Fig. 5, although the reversal is slightly hindered in the case of square dots. This similarity is better understood by looking at the static micromagnetic configuration of the square dots just before the reversal [Fig. 6(a)] [the configuration of a 6-nm-thick dot is also shown in Fig. 6(b) because the so-called nucleation volumes are clearly visible in this case, although the deviation at the edge is obviously too strong for the model to be valid]. Examination of Fig. 6(a) leads to the conclusion that the reversal in the square dots is hindered by the corners, so that the nucleation volumes grow preferentially away from them, in a region which can be locally approximated by a half-infinite slab. This result proves the relevance of the geometric approximation in the case of large square-shaped dots. How large square dots need to be to behave like half-infinite slabs can be probed by repeating such simulations for several edge lengths (Fig. 7). The grid spacing was maintained constant and equal to 3.125 nm for all simulations. This ensures that the exchange field and the stray field were determined with the same precision for each system, and allows us to compare unambiguously all results. Besides, we used the

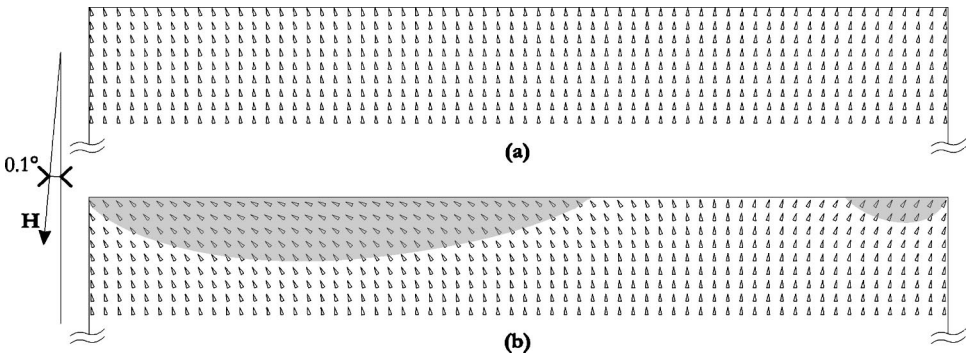

FIG. 6. Near-edge detail of the numerically calculated micromagnetic configuration of 200-nm-square-shaped dots just before reversal. The dot thickness is 1 nm for (a) and 6 nm for (b). The parameters used are $\mu_0 H_a = 0.55$ T and $M_s = 1.73 \times 10^6$ A m^{-1}, which yields $m = 2.81$. The anisotropy field is exactly perpendicular to the edge, whereas a 0.1° misorientation of the applied field was used to trigger symmetry breaking. Areas where spins are rotated by more than 45° are shaded to visualize nucleation volumes.

fftw library developed by Frigs and Johnson.[47] This allowed us to investigate more points than the usual 2^n law with the conventional FFT procedure permits. Indeed, the library of Ref. 47 works equally well for all products of integral powers of prime integers. The results of these simulations are the following. The reversal field goes to the anisotropy field for very small lateral size. This was indeed expected as a small square dot is nearly single domain, and displays no in-plane shape anisotropy. On the contrary, the reversal field of a square dot with a large edge length goes to the reversal field of the half-infinite slab. The crossover to the lateral finite-size effect is found to lie between 100 nm and 200 nm, for the particular case of $H_a = 0.55$ T and $M_s = 1.73 \times 10^6$ A m^{-1}. The reader may note that this is well above all conventional magnetic length scales, such as the exchange length and the domain wall width. We will not discuss the reasons for this in the present article. Finally, the influence of the exact shape of the dot on the reversal field was investigated. This was done by performing simulations on disk-shaped dots 200nm in diameter, yielding results very similar to the case of square dots with identical width and thickness $t = 1$ nm: $\tilde{h}_r = -0.91 \pm 0.005$ in the case of disk-shaped dots, to be compared with $\tilde{h}_r = -0.892 \pm 0.002$ in the case of square-shaped dots discussed above. Therefore, the shape of the dot, at least disk or square, does not seem to be of prime importance in determining the value of $\tilde{h}_r$. This is an indication that the geometric half-infinite approximation may be relevant for different kinds of in-plane shapes. This will be discussed in more detail in Sec. V.

C. Comparison with experiments

The reversible contribution to experimental hysteresis loops of an array of dots is very weak and could not be measured accurately. We therefore restricted the comparison between the analytical model and the numerical calculations to two scalar quantities: the reversal field $\tilde{h}_r$ and the exponent α related to the field dependence of the energy barrier used in the theory of thermal activation.[17]

Let us first discuss the case of the reversal field $\tilde{h}_r$. For 2-nm-thick disk-shaped dots ($H_a = 0.3$ T, Ms$=1.73$ Ms$=1.73\times 106$ A m-1), the experiments yielded $\tilde{h}_r^{\rm expt} = -0.63 \pm 0.01$ whereas the torque model yielded $\tilde{h}_r^{\rm tm} = -0.612 \pm 0.001$. The agreement is rather good in that case. For 1-nm-thick dots $\tilde{h}_r^{\rm expt} = -0.733 \pm 0.005$ (Ref. 40) and $\tilde{h}_r^{\rm tm} = -0.857 \pm 0.001$. Both results do not coincide. The discrepancy is not very large in terms of reversal field values but as we pointed out in the introduction $\Delta\tilde{h} = 1 + \tilde{h}$ is a direct probe of self-demagnetizing effects in dots. $\Delta\tilde{h}_r^{\rm expt} = 0.267 \pm 0.005$ and $\Delta\tilde{h}_r^{\rm tm} = 0.143 \pm 0.001$ are therefore the relevant parameters to be compared. The agreement is worse viewed from this angle. We ascribed this discrepancy to dot defects, which indeed are expected to have more dramatic consequences in thinner dots for two reasons:

(i) A roughnesslike fluctuation of the number of Fe atomic planes in the dot. Two physical effects are related to thickness fluctuations, and both effects add up. Indeed, if the dot thickness near an edge is locally increased, the anisotropy is decreased and the demagnetizing fields are increased, so that both effects tend to decrease $|\tilde{h}_r|$. It should be noted that this effect is more important for thinner dots in terms of

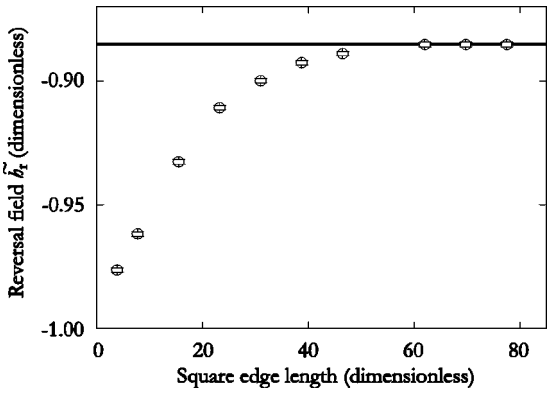

FIG. 7. Numerically simulated dimensionless reversal field of a square dot, as a function of the side length. The line shows the numerically simulated reversal field of a half-infinite slab. The dimensionless parameters are magnetization $m = 2.81$ and thickness $t = 0.15$. Let us recall that the dimensionless unit length equals 6.5 nm for iron when $H_a = 0.55$ T.

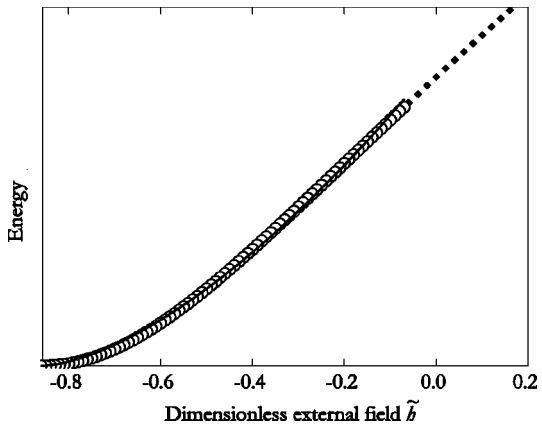

FIG. 8. Energy barrier height as a function of the applied field, as predicted by the model. The example shown corresponds to the experimental parameters of 1-nm-thick dots. The curve was fitted with an adjustable activation volume and exponent α (straight line). Open dots stand for the energy range taken into account in the fit, whereas solid diamonds stand for points excluded from the fit.

relative values.[48] For instance, 1-nm dots contain on the average 5 monolayers (ML) of Fe, so that large relative thickness fluctuations are simply induced by the fluctuation of the position of atomic steps at both Mo/Fe interfaces, even in the case of an atomically flat and roughness-free sample, because of the substrate miscut. This may explain why the model reproduces well the reversal of 2-nm-thick dots and poorly that of 1-nm-thick dots.

(ii) $\tilde{h}_r$ is very close to -1 so that the energy well is very shallow and narrow just before the reversal,[25] and even small defects are expected to play a considerable role.

Let us now discuss the case of exponent α. The analysis of the experimental thermal activation data was performed between 2 K and 300 K on 1-nm-thick dots. The procedure was the following. In a first step, the value of $\tilde{h}_r$ was measured in this temperature range. In a second step, the decrease of $\tilde{h}_r$ with increasing temperature was ascribed to thermal activation, which helps overcoming the field-dependant energy barrier $\Delta(\tilde{h}_r)$. An Arrhenius law was used to describe thermal activation, and thus for each temperature the height of the energy barrier at $\tilde{h}$ was estimated, yielding $\Delta(\tilde{h})$. As a third and final step, this experimental $\Delta(\tilde{h})$ curve was fitted by the following expression: $\Delta_0[\tilde{h}_r(T)-\tilde{h}_r(T=0)]^\alpha$. This procedure yielded $\alpha=1.65\pm0.1$.[25] On the other hand, given the dot parameters, the model predicts that the dot is single domain and therefore that $\alpha_{SD}=2$. However, α_{SD} cannot be compared directly with experiments as it arises from a lowest-order expansion of Eq. (28), which is in the limit of zero temperature. One must instead compare the exponent issued from experiments with the exponent issued from a polynomial fit of Eq. (28) over the field range $[\tilde{h}_r(300\text{ K}),\tilde{h}_r(2\text{ K})]$. This field range is the one probed experimentally using the temperature range [2 K, 300 K]. The fitting procedure is illustrated in Fig. 8 and yields $\alpha_{SD}^{2-300\text{ K}}=1.56\pm0.02$. The torque model is therefore in good agreement with experiment. Experimental determination of the exponent α_{NU} in the case of thicker dots and its comparison with the model would, however, be required to fully validate the model. Besides, thermal activation theories are derived from the effect of thermal noise on a single degree of freedom,[49] i.e., are in principle applicable only to single-domain systems. The Arrhenius law and Brown equations may therefore not be directly applicable to the case of a functional degree of freedom, as it is the case in the torque model and in the majority of magnetic systems, which are not necessarily in a single domain state. One has therefore to keep in mind that there are no absolutely firm bases to make such comparisons.

V. DISCUSSION

A. Validity domain of the model

Let us first discuss the limit of validity of the model in terms of maximum tractable thickness. We showed in the previous section that in the low-thickness regime the model and numerical simulations predicted very similar values for $1+\tilde{h}$ (the reduction of the reversal field as compared to the anisotropy field). Nevertheless, the value predicted by the model saturates above approximately $t=0.5$, whereas that yielded by numerical calculations still increases slowly. This can be understood as volume charges were neglected in the model so that only surface charges (i.e., on the edges) contribute to demagnetizing effects. The higher the thickness is, the larger ω_0^r is, so that surface charges and therefore the associated demagnetizing effects are smaller. In real dots and in numerical calculations, part of the demagnetizing effect in that case is still taken into account via volume charges. This might explain why $1+\tilde{h}$ still increases slowly. Let us discuss the situation quantitatively. In the limit of large thickness $\omega_0^r\to\pi/2$, so that surface charges nearly vanish [due to power expansion of $\cos(\omega_0)$ function in Eq. (20), $\omega_0^r\to\sim1.59$ in the model, instead of $\pi/2$]. In this case the reversal is hindered by the exchange torque only, whereas no more demagnetizing torque applies. Thus, the reversal finally occurs for $\Gamma_{ex}=0$, i.e., $\tilde{h}\sim-0.62$ [this comes out of Eq. (9)]. It is indeed checked in Fig. 4 that magnetization saturation is related to $\tilde{h}$ approaching -0.60. We also observe on this plot that this limit is obtained for $t\approx0.5\approx0.3\lambda_{ex}$. This also can be understood as we already mentioned that demagnetizing effects are significant only on a lateral length scale of the order of the dot thickness t. Indeed λ_{ex} is the length scale that arises when exchange (A) and demagnetizing effects due to *two* charged planes ($m^2/2$) compete. In our case λ_{ex} is obviously the minimum length scale of the activation volume as $\lambda_{ex}<\lambda_{Bl}$. As long as $t\ll\lambda_{ex}$ the mean demagnetizing energy over the nucleation volume is well below $m^2/2$. In other words the charged edge of the dot does not look like a plane, as viewed from the nucleation volume. In that case the reversal is mainly made possible by Zeeman energy only. The crossover between Zeeman-driven reversal to dipolar-driven reversal therefore logically occurs around $t\sim\lambda_{ex}$. This length scale is also the thickness over which the torque model is no longer relevant.

Let us now discuss the predicted size of nucleation volumes. Below the crossover thickness mentioned above, the influence of dipolar fields can be considered as pinpointlike as compared to V_n. The characteristic length scale of nucleation volumes in the direction perpendicular to the edge is therefore determined by Eq. (6) and is not expected to depend much on the demagnetizing field magnitude. In other words, and provided that the thickness of the dot is reasonably smaller than the exchange length, the relevant in-plane length scale in the direction perpendicular to the edge is not the exchange length but is rather determined by a portion of a wall described by Eq. (6). This length is somewhat larger than λ_{ex}, but anyhow differs from the Bloch-wall width. This illustrates the fact that neither the maximum nor the minimum of λ_{ex} and λ_{Bl} is a universal magnetic characteristic length scale for all systems. However, it is clear from Eq. (6) that this length scale increases with decreasing anisotropy. However, as long as the uniaxial anisotropy is strong enough, the length scale of the nucleation volumes perpendicular to the edge does not depend on the dot size. This is the reason why we call the reversal ''non-collective'': the effect of the demagnetizing fields is concentrated in areas close to the edges, and the magnetization reversal does not involve all the spins of the system. On the contrary, in the limit of zero microscopic anisotropy, i.e., for soft materials, this length scale diverges and the nonuniform volume fills the entire dot. In that case the magnetization state of a soft dot can be called ''collective,'' and can be accurately described using length variables scaled with dot size and low-order expansions performed from the center of the dot.[36] To this point, an important remark must be made. Figure 2 shows that, in the limit of small thickness, H_r goes to the value predicted for coherent reversal. However, as pointed out above, the magnetization reversal is not collective. These two statements do not contradict each other. They are explained by the fact that, although the reversal is not coherent, the conditions in the vicinity of the nucleation volume are very similar to those needed for coherent reversal (in our case, nearly vanishing dipolar fields), so that the field at which the nucleation volume reverses is close to that predicted by the Stoner-Wohlfarth theory. The fact that the reversal is *not* coherent was checked directly by inspection of the dynamics of the numerically simulated reversal. The reversal is clearly initiated near the edge and propagates into the dot through domain-wall motion. This shows that, in the case of a real systems, one cannot conclude that coherent reversal occurs simply on account of the similarity of an experimental $H_r(\theta)$ reversal law with the so-called Stoner-Wohlfarth Astroïd. The definite proof must come from dynamical measurements, which allows one to estimate the size of nucleation volumes.[17]

Let us finally discuss the influence of the dot shape on reversal. In the case of flat dots made of soft material it was shown experimentally[50,51] and numerically[51,52] that the micromagnetic configuration and the reversal field value strongly depend on the exact shape of the edges. This is explained by the fact, explained above, that the nonuniform magnetization state fills the entire dot for soft materials. Therefore, the influence of the edges is in this case long ranged. To the contrary, in dots made of hard materials the nucleation volumes are mainly influenced by the *local* shape and orientation of the nearby edge. If all edge orientations are available as in the case of disks, the relevance of the geometric hypothesis indicates that the highest reversal field (speaking of negative values, ie., the smallest in absolute value) is associated with edges that are exactly perpendicular to the easy axis. This means that the torque model should be relevant to describe thin and flat dots made of hard material with in-plane anisotropy, and this for a large variety of in-plane geometry of dots, provided that a significant part of their edges is perpendicular to the easy axis. What a ''significant part'' is was probed by numerical calculations in Sec. IV B, and is a length scale expected to increase with decreasing anisotropy, Fig. 7. This lateral length scale is about 50–100 nm for 1-nm-thick dots, and was found to be about 1–2 μm in dots with a much weaker bulk Fe fourth-order anisotropy.[53]

Following this discussion, it appears that the model is well suited to describe dots with in-plane uniaxial anisotropy, of thickness smaller than about half the exchange length, of lateral size much larger than the exchange length and the domain-wall width, and with a significant portion of their edges perpendicular to the easy axis of magnetization. To the contrary, the best suited method applicable to very small dots would be a variational method as the one introduced by Cowburn and Welland,[36] used to describe a close-to-uniformly-magnetized state.

B. Compliance with general micromagnetic statements

General micromagnetic theorems or statements are often invoked regarding some aspects of magnetization reversal. Let us check in this section that the results of the present model comply with them. We discuss successively the relevance of a single-domain (SD) state and that of the numerical value of exponent α.

A key prediction of our model is that the magnetization configuration is uniform above a given external applied field. With the parameters of our Fe dots[25] this field is negative, which means that the magnetization configuration is uniform for $h=0$. Besides, the predicted configuration is always uniform below a critical thickness, whatever the external field is. These predictions were confirmed by numerical calculations (see Fig. 9). The occurrence of a perfectly uniform magnetization state in a half-infinite slab may be surprising at first glance. Indeed it is well known that the only systems that may be uniformly magnetized under a finite external field are those bounded by a surface with a polynomial equation whose degree is at most equal to two[54,55]: ellipsoids, paraboloids, hyperboloids, cylinders, and slabs. In particular, the magnetization is never uniform in the vicinity of edges or corners, because of the logarithmic divergence of dipolar fields.[41] Despite the two sharp edges of a half-infinite slab, we can get a uniform magnetization in our model because of one hypothesis we made: the magnetization direction is uniform throughout the thickness of the slab and is maintained in the plane of the film. We are therefore put back to a perfectly 2D system, whose single edge is a line (the 2D

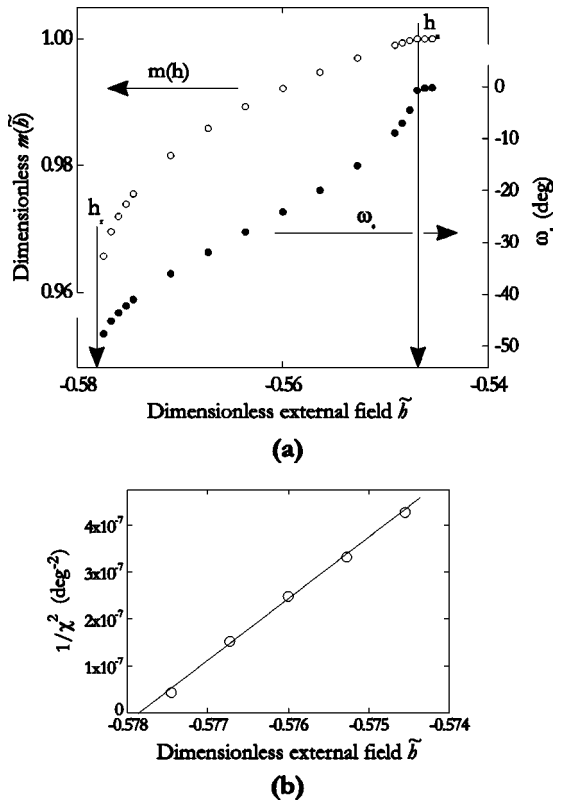

FIG. 9. (a) Detail of the numerically simulated hysteresis loop $m(h)$ and spin angle ω_0 at the edge of a half-infinite flat dot with translation symmetry parallel to the edge. The parameters used were $m=2.81$ and $e=4$ nm (points with the largest thickness in Fig. 4). (b) Squared inverse of susceptibility $\chi=d\omega_0/dh$ in the vicinity of the reversal field, for the same sample.

analogy of a 3D surface) and is therefore of first order. Besides, the dipolar fields do not diverge in the vicinity of the edge, due to their averaging over the slab thickness.[41] Finally, as the edge is exactly perpendicular to the easy axis of magnetization, the symmetry of the Brown condition (the Euler equation at the very edge) and that of the anisotropy plus Zeeman energy 2D dot are identical (the field is applied exactly perpendicular to the edge), so that the slab may be uniformly magnetized. Therefore, the predictions of the model do not contradict the micromagnetic theory of uniform magnetization. Note that, however, in the case of a real finite-size dot (even defect free), it is most probable that no component of the magnetization is uniform, because of corners and edge orientations other than parallel or perpendicular to the external field and anisotropy axis.

Let us now discuss the predictions of the numerical values of exponent α. Two statements can be inferred from the model. First, $\alpha_{SD}=2$ and $\alpha_{NU}=1.5$ remind us of the exponents derived in the framework of coherent rotation: $\alpha=2$ when the external field is applied exactly along the easy axis, i.e., when **m** and **h** are always collinear, whereas $\alpha=1.5$ when the external applied field is applied at an angle away from the easy axis, i.e., when **m** and **h** are not collinear.[56] Second, our model emphasizes that the numerical values of α given above are relevant only for first-order expansions and that the field dependence of the energy barrier is generally not a polynomial law. The law is polynomial for neither α_{SD} nor α_{NU} in the present model. Indeed these are exponents of the leading term of a series expansion of the energy barrier, which is not an exact polynomial function of $\tilde{h}_r - \tilde{h}_r(T=0)$. In the theory of coherent rotation,[26] for noncollinear **m** and **h** the law is also nonpolynomial, whereas in the collinear case the energy barrier field dependence is exactly parabolic. Therefore, there is not a full analogy between CR and the present model. The experimental consequences are twofold. First, it is not incorrect to find experimental exponents different from 2 or 1.5 for nucleation events, or even to find that the energy barrier dependence is not polynomial. Second—and this is a direct corollary of the first statement—the exponent α yielded by fitting the energy barrier dependence issued from experimental data depends on the investigated energy barrier range. Consequently one should be careful to compare α exponents issued from analyses carried out over the same energy barrier range, as we did on Sec. IV C.

C. Parallel with a Landau-like energy

Phase transitions are often described by expanding the free energy of a system in the vicinity of the transition, leading to a so-called Landau energy. In the simplest case only terms with even integral powers of the order parameter ω_0 are considered:

$$e = a\omega_0^2 + b\omega_0^4 + c\omega_0^6. \tag{32}$$

This energy is obtained in our case by the torques given by Eqs. (9) and (22). The link with Eqs. (23) and (24) is $a=C$, $b=B/2$, and $c=A/3$. We focus below on magnetization reversal processes at $T=0$K, which means that metastability is maximum, and the reversal is determined by the disappearance of the local minimum. In this case and using the Landau-energy framework, the reversal occurs when a changes its sign. The variation of the ''order parameter'' ω_0 across the reversal is discontinuous for $b<0$ and continuous for $b>0$. The discontinuity is the signature of the nonreversed SD state to reversed SD event, whereas the continuity is associated with the SD-to-NU state event. Therefore, in our case the change of the sign of b with the condition $a=0$ determines the critical thickness t_c below which the dot is always in a single-domain state. Besides, above t_c the reversal field $\tilde{h}_r$ depends on the value of c.

Some general features of a phase transition can be predicted once the expansion of the free energy is performed. Systems described by similar expansions have identical critical exponents—they belong to the same *class of universality*. It is straightforwardly derived from Eq. (32) that the order parameter ω_0 grows with a power 1/2 after a second-order transition occurs. In the context of the model this is expressed as $\omega_0^2 \sim h_n - h$. It can be shown that the critical exponent is 1/2 before h_r as well, i.e., that $(\omega_0 - \omega_0^{max})^2 \sim h - h_r$ (this can also be checked numerically from the data of Fig. 2). The prediction of these exponents has been made possible by the approximations of the model, which restricted the problem to a self-consistent equation with one

parameter only. Without these approximations, the class of universality of a real dot with nonuniform magnetization cannot be predicted straightforwardly because of the large number of degrees of freedom involved. We used numerical calculation to gain insight into the behavior of such more realistic dots. We derived critical exponents in the case of a simulated half-infinite slab with a translation symmetry parallel to the edge (see Sec. IV B). The simulated loops used to derive these exponents are the same that were used to derive the simulated phase diagram in Fig. 4 [see Fig. 9(a)]. From these curves, we shall find for $\tilde{h}_r$ and $\tilde{h}_n$ the exponent β such that $\omega_0(h)-\omega_0(h_c)\sim(h-h_c)^\beta$ (h_c is h_r or h_n). In the case of nucleation, $\omega_0(h_n)=0$, so that $\omega_0(h)\sim(h-h_n)^\beta$. Besides, ω_0 is close to zero in the vicinity of h_n, so that $m\sim 1-\omega_0^2/2\sim(h-h_n)^{2\beta}$. A close inspection of Fig. 9(a) reveals that m varies linearly with h in the vicinity of h_n. Thus, we deduce $\beta=1/2$ for nucleation. The case of reversal of a NU state is more difficult to handle, as the nonzero value of $\omega_0(h_r)\neq 0$ has to be extrapolated from simulations just before the reversal, which may induce errors in the evaluation of β. Instead we used a procedure based on the evaluation of the susceptibility $dm/d\tilde{h}$. It can be shown straightforwardly that $1/\chi^2\sim(h-h_c)^{2(1-\beta)}$. We check in Fig. 9(b) that $1/\chi^2$ varies linearly with h in the vicinity of h_r, which proves that $\beta=1/2$. Therefore, the critical exponent β equals exactly 1/2 in the vicinity of both h_n and h_r, i.e., exactly the same value as in the simplified case of the torque model. This indicates that the hypotheses made in the framework of the analytical model do not prevent the qualitative behavior of dots to be predicted. The simulated prediction of exponents 1/2 does not seem to be related to the present restrictive geometry (1D set of degrees of freedom) as an exponent 1/2 was also found during the onset of reversal in 3D ferromagnetic cubes.[57]

D. Simplified forms of the results

We shall now make use of the analogy developed in the previous paragraph, in order to derive an approaching scaling law for the nucleation field in the limit of low thickness. In this limit, $h_n=h_r$ is determined by the cancellation of a, which leads to the following equation [Eqs. (15)–(19) and (24)]:

$$-\ln\left(\frac{t}{2}\sqrt{1+\tilde{h}}\right)=C-1+\frac{4\pi}{m^2 t}\sqrt{1+\tilde{h}}, \tag{33}$$

where C is Euler's constant. The above logarithm function prevents any exact polynomial scaling law from being derived for $1+\tilde{h}_n$. However, as $\sqrt{1+\tilde{h}}$ goes to zero when t goes to zero, the left-hand side of Eq. (33) diverges, so that t is negligible before $\sqrt{1+\tilde{h}}$. More precisely, $\sqrt{1+\tilde{h}}$ is negligible before any function $t^{\alpha/2}$ for $\alpha/2<1$, in the limit of $t\to 0$. Phenomenologically, $1+\tilde{h}$ behaves locally like t^α, with α being smaller than 2, but closer and closer to 2 when t goes to zero. Plotting $1+\tilde{h}$ as a function of t in a log-log scale reveals that α is very close to 1.5 in a broad range of m values, for $t>0.02$ and $\tilde{h}_r$ below approximately 0.2 (Fig. 10): $(1+\tilde{h})\sim t^{3/2}$. As a matter of fact, $(1+\tilde{h})/t^{3/2}$ slightly decreases with t, as shown in the inset of Fig. 10. Taking into account this slight slope, we could derive the following phenomenological expression from fits for various m values:

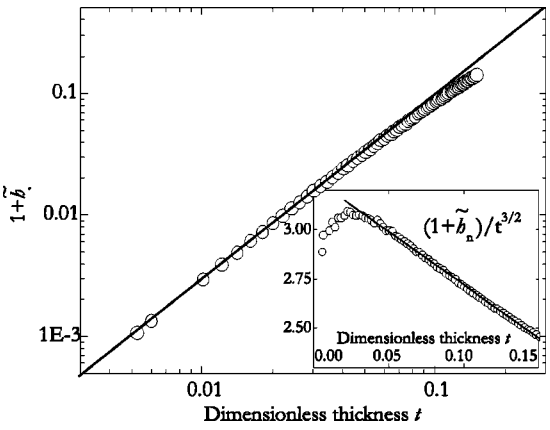

FIG. 10. Log-log plot of $1+\tilde{h}_n$ as a function of dimensionless thickness t, for $m=2.81$. The slope of the line is exactly 3/2. Inset: $(1+\tilde{h}_n)/t^{3/2}$ as a function of t, showing a weakly thickness-dependent value. The line is the result of a linear fit for thickness above 0.03.

$$1+\tilde{h}_n\simeq 0.0873 m^{7/2} t^{3/2}(1-0.596 mt) \tag{34}$$

or, expressed in SI units,

$$1-\left|\frac{H}{H_a}\right|\simeq 0.0873\left(\sqrt{\frac{\mu_0 M_s^2}{A}}\right)^{7/2}\left(\frac{A}{K}\right)^2 T^{3/2} \times\left(1-0.596T\sqrt{\frac{\mu_0 M_s^2}{A}}\right). \tag{35}$$

Equation 35 is accurate within a few percent in the range $m\in[1.5,6]$ and $\tilde{h}<-0.75$, and can be used for a quick evaluation of $\tilde{h}_n$. Let us finally recall the reader that very often K originates mainly, in interface anisotropy in the ultrathin regime, following the phenomenological law $K\sim K_s/T$,[58] so that $1+|H/H_a|$ is expected to scale with $T^{5/2}$ in that case.

We end the discussion by clarifying a discrepancy that may appear with previously published results. Indeed, we shortly mentioned the principle and basic outputs of the present model in a Letter.[25] The formulas given in Ref. 25 are much simpler than those given here. This is due to the fact that we previously did not make a full expansion of all equations up to ω_0^6. Instead, we considered for the coefficients of each power only the leading terms, in the limit of small thickness. We shall not give the details of these approximations here, but it can be checked in Fig. 11 that the crude version of Ref. 25 and the present model yield identical results in a reasonable range of low thickness. The agreement is found to be better for smaller dimensionless magnetization m.

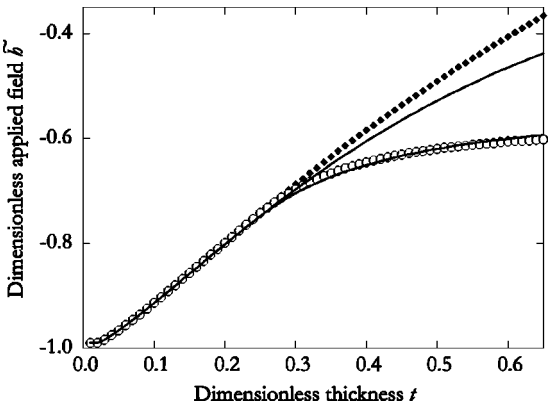

FIG. 11. Predictions of the present model for $\tilde{h}_n$ (solid diamonds) and $\tilde{h}_r$ (open dots). The lines show the values predicted by the simplified formulas given in Ref. 25. We used magnetization $m=2.81$ in the calculations.

VI. CONCLUSION

In the case of flat dots with in-plane uniaxial anisotropy and lateral dimensions well above the exchange length λ_{ex} and the domain wall width λ_{wall}, magnetization reversal occurs by a localized nucleation event followed by a fast wall propagation. In the literature the reversal field is often predicted by assuming that coherent rotation occurs in a phenomenological nucleation volume V_n. The effect of the dipolar field acting on V_n is then often estimated by calculating the aspect ratio of an approaching geometry of the dot, which is related to the average dipolar energy over the whole dot. This approach is not valid because (1) dipolar fields are highly nonhomogeneous in a uniformly magnetized flat dot and (2) exchange forces are neglected.

We proposed in this article an analytical model specific to ultrathin flat dots with in-plane uniaxial anisotropy, which takes into account these two aspects. The major approximations of the model are the following: (1) The geometry is simplified to a half-infinite slab with a linear infinite edge perpendicular to the easy axis of magnetization. (2) The demagnetizing effects are taken into account as a pinpoint torque applied at the edge. Under these assumptions we derived analytical equations for the field-dependent configuration of the nucleation volume. The reversal field $\tilde{h}_r$ and the exponent α associated with the field dependence of the energy barrier preventing reversal are predicted. $|\tilde{h}_r|$ is found to decrease with either increasing thickness T or increasing volume magnetization M_s, or decreasing anisotropy K. Below a critical thickness the static configuration of the slab is predicted to be always single domain (i.e., perfectly uniformly magnetized) whatever $\tilde{h}$ is, and $\alpha=2$. Above this critical thickness a nucleation field $\tilde{h}_n$ is also derived with $|\tilde{h}_n| < |\tilde{h}_r|$, and $\alpha=1.5$. In the limit of small thickness, the following approached scaling law is found: $1-|H_r/H_a| \sim M_s^{7/2}A^{-3/4}K^{-1}T^{3/2}$, where A is the exchange stiffness and H_a is the anisotropy field, i.e., the reversal field predicted for coherent reversal. It must be noted that H_r goes toward H_a although the reversal is demonstrated to be not coherent. This emphasizes that the measure of an experimental astroïd-like $H_r(\theta)$ is not sufficient alone to conclude that coherent reversal indeed occurs in a real system.

All model predictions are in good quantitative agreement with numerical calculations and/or experiments. Numerical calculations also showed that $\tilde{h}_r$ does not depend much on the particle shape or size, contrary to what is usually found for dots made of soft material. It follows from this and from the more detailed discussion in the paper that this model should be a simple and reliable tool to investigate and predict characteristics of magnetization reversal processes in thin flat dots with a uniaxial in-plane anisotropy, provided that the following conditions are simultaneously fulfilled: (1) the thickness of the dots is much smaller than the exchange length, (2) the lateral size of the dots is well above λ_{ex} and λ_{wall}, and (3) a significant part of the dot edge is approximately linear and roughly perpendicular to the easy axis of magnetization. A ''significant part'' is to be compared with several times λ_{ex} and λ_{wall}. Finally, (4) the hysteresis loop is performed along the easy axis of magnetization.

ACKNOWLEDGMENTS

We are grateful to Pr. Gradmann (MPI Halle, Germany) for stimulating discussions and for a thorough and critical reading of the manuscript.

*Corresponding author. Electronic address: fruch@polycnrs-gre.fr

[1] F. J. Himpsel, J. E. Ortega, G. J. Mankey, and R. F. Willis, Adv. Phys. **47**, 511 (1998).

[2] *Magnetic Ultrathin Films, Multilayers and Surfaces*, edited by A. Fert, H. Fujimori, G. Guntherodt, B. Heinrich, W. F. Egelhoff, Jr., E. E. Marinero, H. Fujimori, and R. L. White, MRS Symposia Proceedings No. 384 (Materials Research Society, Pittsburgh, 1995).

[3] *Ultrathin Magnetic Structures*, edited by J. A. C. Bland and B. Heinrich (Springer-Verlag, Berlin, 1994).

[4] *Magnetism and Structure in Systems of Reduced Dimensions*, Vol. 309 of *NATO Advanced Study Institute*, *Series B: Physics*, edited by R. F. C. Farrow, B. Dieny, M. Donath, A. Fert, and B. D. Hermsmeier (Plenum Press, New York, 1993).

[5] M. S. Wei and Y. S. Chou, J. Appl. Phys. **76**, 6679 (1994).

[6] W. Wernsdorfer, B. Doudin, D. Mailly, K. Hasselbach, A. Benoit, J. Meier, J.-P. Ansermet, and B. Barbara, Phys. Rev. Lett. **77**, 1873 (1996).

[7] L. Ressier, A. Schuhl, F. N. V. Dau, K. Postava, M. Goiran, J. P. Peyrade, and A. R. Fert, J. Appl. Phys. **81**, 5464 (1997).

[8] A. Sugawara, G. G. Hembree, and M. R. Scheinfein, J. Appl. Phys. **82**, 5662 (1997).

[9] J. Hauschild, U. Gradmann, and H. J. Elmers, Appl. Phys. Lett. **72**, 3211 (1998).

[10] B. Voigtländer, G. Meyer, and N. M. Amer, Phys. Rev. B **44**, 10 354 (1991).

[11] S. Y. Chou, M. S. Wei, and P. B. Fischer, IEEE Trans. Magn. **MAG-30**, 4485 (1994).

[12] W. Wernsdorfer, K. Hasselbach, D. Mailly, B. Barbara, A. Benoit, L. Thomas, and G. Suran, J. Magn. Magn. Mater. **145**,

33 (1995).
[13] N. Bardou, B. Bartenlian, C. Chappert, R. Mégy, P. Veillet, J. P. Renard, F. Rousseaux, M. F. Ravet, J. P. Jamet, and P. Meyer, J. Appl. Phys. **79**, 5848 (1996).
[14] M. Hehn, K. Ounadjela, J. P. Bucher, F. Rousseaux, D. Decanini, B. Bartenlian, and C. Chappert, Science **272**, 1782 (1996).
[15] L. Ressier, J. Diaz, and J. P. Peyrade, Appl. Phys. Lett. **70**, 2195 (1997).
[16] P. R. Krauss and S. Y. Chou, Appl. Phys. Lett. **71**, 3174 (1997).
[17] W. Wernsdorfer, E. B. Orozco, K. Hasselbach, A. Benoit, B. Barbara, N. Demoncy, A. Loiseau, H. Pascard, and D. Mailly, Phys. Rev. Lett. **78**, 1791 (1997).
[18] M. Sussiau, F. Nguyen-Van-Dau, P. Galtier, and A. Schuhl, Appl. Phys. Lett. **69**, 857 (1996).
[19] U. Gradmann, T. Dürkop, and H. J. Elmers, J. Magn. Magn. Mater. **165**, 56 (1997).
[20] L. F. Schelp, A. Fert, F. Fettar, P. Holody, S. F. Lee, J. L. Maurice, F. Petroff, and A. Vaures, Phys. Rev. B **56**, R5747 (1997).
[21] Y. Lu, R. A. Altman, A. Marley, S. A. Rishton, P. L. Trouillard, G. Xiao, W. J. Gallaghev, and S. S. P. Parkin, Appl. Phys. Lett. **70**, 2610 (1997).
[22] R. L. White, Data Storage **4**, 55 (1997).
[23] O. Fruchart, J.-P. Nozières, B. Kevorkian, J.-C. Toussaint, D. Givord, F. Rousseaux, D. Decanini, and F. Carcenac, Phys. Rev. B **57**, 2596 (1998).
[24] J.-E. Wegrowe, O. Fruchart, J.-P. Nozières, D. Givord, F. Rousseaux, and D. Decanini, J. Appl. Phys. **86**, 1028 (1999).
[25] O. Fruchart, J.-P. Nozières, W. Wernsdorfer, D. Givord, F. Rousseaux, and D. Decanini, Phys. Rev. Lett. **82**, 1305 (1999).
[26] L. Néel, C. R. Acad. Sci. **224**, 1550 (1947).
[27] E. C. Stoner and E. P. Wohlfarth, Philos. Trans. R. Soc. London, Ser. A **240**, 599 (1948).
[28] M. Rührig, W. Bartsch, M. Vieth, and A. Hubert, IEEE Trans. Magn. **MAG-26**, 2807 (1990).
[29] W. F. J. Brown, Phys. Rev. **105**, 1479 (1957).
[30] E. H. Frei, S. Shtrikman, and D. Treves, Phys. Rev. **106**, 446 (1957).
[31] A. Aharoni and S. Shtrikman, Phys. Rev. **109**, 1522 (1958).
[32] A. Aharoni, Phys. Status Solidi **16**, 3 (1966).
[33] H. A. M. V. den Berg, J. Magn. Magn. Mater. **44**, 207 (1984).
[34] H. A. M. V. den Berg, J. Appl. Phys. **60**, 1104 (1986).
[35] P. Bryant and H. Suhl, Appl. Phys. Lett. **54**, 78 (1989).
[36] R. P. Cowburn and M. E. Welland, Phys. Rev. B **58**, 9217 (1998).
[37] R. P. Cowburn and M. E. Welland, J. Appl. Phys. **86**, 1035 (1999).
[38] S. T. Chui and V. N. Ryzhov, Phys. Rev. Lett. **78**, 2224 (1997).
[39] W. Wernsdorfer, K. Hasselbach, A. Benoit, G. Cernicchiaro, D. Mailly, B. Barbara, and L. Thomas, J. Magn. Magn. Mater. **151**, 38 (1995).
[40] O. Fruchart, W. Wernsdorfer, J.-P. Nozières, D. Givord, F. Rousseaux, D. Mailly, D. Decanini, and F. Carcenac, J. Magn. Magn. Mater. **198-199**, 228 (1999).
[41] W. Rave, K. Ramstöck, and A. Hubert, J. Magn. Magn. Mater. **183**, 329 (1998).
[42] A. Aharoni, Phys. Rev. **119**, 127 (1960).
[43] H. Träuble, O. Boser, H. Kronmüller, and A. Seeger, Phys. Solid State **10**, 283 (1965).
[44] I. S. Gradshteyn and I. M. Ryzhik, *Table of Integrals, Series, and Products*, 5th ed. (Academic Press, London, 1994).
[45] A. Aharoni, IEEE Trans. Magn. **MAG-22**, 478 (1986).
[46] J.-C. Toussaint, B. Kevorkian, O. Fruchart, and J. Voiron, in *Proceedings of the Tenth International Symposium on Magnetic Anisotropy and Coercivity in Rare-Earth Transition Metal Alloys, Dresden, Germany, 1998* (Werkstoff-Informationgesellschaft, Francfort, Germany, 1998).
[47] We used the fast Fourier transform procedure developed by M. Frigs and S. G. Johnson, that is able to handle meshes with a number of cells equaling an arbitrary product of prime integers, not only powers of 2 (http://www.fftw.org).
[48] O. Fruchart, J.-P. Nozières, and D. Givord, J. Magn. Magn. Mater. **207**, 146 (1999).
[49] W. F. J. Brown, Phys. Rev. **130**, 1677 (1963).
[50] K. J. Kirk, J. N. Chapman, and C. D. W. Wilkinson, Appl. Phys. Lett. **71**, 539 (1997).
[51] J. Shi, T. Zhu, M. Durlam, S. Tehrani, Y. F. Zheng, and J.-G. Zhu, IEEE Trans. Magn. **MAG-34**, 997 (1998).
[52] J. Gadbois, J.-G. Zhu, W. Vavra, and A. Hurst, IEEE Trans. Magn. **MAG-34**, 1066 (1998).
[53] Y. B. Xu, A. Hirohata, L. Lopez-Diaz, H. T. Leung, M. Tselepi, S. M. Gardiner, W. Y. Lee, J. A. C. Bland, F. Rousseaux, E. Cambril, and H. Launois, J. Appl. Phys. **87**, 7019 (2000).
[54] J. C. Maxwell, *A Treatise on Electricity and Magnetism*, 3rd ed. (Clarendon, Oxford, 1872), Vol. 2, pp. 66–73.
[55] J. A. Osborn, Phys. Rev. **67**, 351 (1945).
[56] R. H. Victora, Phys. Rev. Lett. **63**, 457 (1989).
[57] A. Hubert and W. Rave, Phys. Status Solidi B **211**, S815 (1999).
[58] P. Bruno, J. Appl. Phys. **64**, 3153 (1988).